Unfolded protein response activation reduces secretion and extracellular aggregation of amyloidogenic immunoglobulin light chain

Christina B. Cooley[a,b,1], Lisa M. Ryno[a,b,1], Lars Plate[a,b], Gareth J. Morgan[a,b], John D. Hulleman[a,b,2], Jeffery W. Kelly[a,b,c,3], and R. Luke Wiseman[b,d,3]

Departments of [a]Chemistry, [b]Molecular and Experimental Medicine, and [d]Chemical Physiology, and [c]The Skaggs Institute for Chemical Biology, The Scripps Research Institute, La Jolla, CA 92037

Edited by F. Ulrich Hartl, Max Planck Institute of Chemistry, Martinsried, Germany, and approved July 30, 2014 (received for review April 2, 2014)

Light-chain amyloidosis (AL) is a degenerative disease characterized by the extracellular aggregation of a destabilized amyloidogenic Ig light chain (LC) secreted from a clonally expanded plasma cell. Current treatments for AL revolve around ablating the cancer plasma cell population using chemotherapy regimens. Unfortunately, this approach is limited to the ∼70% of patients who do not exhibit significant organ proteotoxicity and can tolerate chemotherapy. Thus, identifying new therapeutic strategies to alleviate LC organ proteotoxicity should allow AL patients with significant cardiac and/or renal involvement to subsequently tolerate established chemotherapy treatments. Using a small-molecule screening approach, the unfolded protein response (UPR) was identified as a cellular signaling pathway whose activation selectively attenuates secretion of amyloidogenic LC, while not affecting secretion of a nonamyloidogenic LC. Activation of the UPR-associated transcription factors XBP1s and/or ATF6 in the absence of stress recapitulates the selective decrease in amyloidogenic LC secretion by remodeling the endoplasmic reticulum proteostasis network. Stress-independent activation of XBP1s, or especially ATF6, also attenuates extracellular aggregation of amyloidogenic LC into soluble aggregates. Collectively, our results show that stress-independent activation of these adaptive UPR transcription factors offers a therapeutic strategy to reduce proteotoxicity associated with LC aggregation.

ER proteostasis | amyloid

Light-chain amyloidosis (AL) afflicts 8–10 people per million per year, making it the most prominent systemic amyloid disease (1). AL is a gain-of-toxic function disease driven by a clonally expanded plasma cell that secretes amyloidogenic Ig light chains (LCs). These amyloidogenic LCs undergo extracellular misfolding and aggregation into proteotoxic soluble oligomers and amyloid fibrils that interact with distal tissues such as the kidney, heart, and gastrointestinal tract, leading to organ dysfunction and ultimately death by unknown proteotoxicity mechanism(s) (2).

The majority of AL patients must combat both a cancer (i.e., the clonally expanded plasma cell) and LC aggregation-associated proteotoxicity. The standard treatment for AL patients is chemotherapy (often combined with stem cell transplant) to eliminate the cancerous plasma cell population (3, 4). The proteasome inhibitor bortezomib, which takes advantage of the stress sensitivity of aggressively proliferating plasma cells, has transformed chemotherapy effectiveness (5–7). Regardless, ∼30% of AL patients with substantial cardiac or renal LC proteotoxicity are too ill at diagnosis to tolerate chemotherapeutics (8–10). Thus, new strategies to reduce LC organ proteotoxicity must be developed to allow more AL patients to take advantage of chemotherapy.

LC aggregation requires conformational changes and a sufficient concentration of misfolded LC in plasma, which determine the rate and extent of its concentration-dependent aggregation. Over 500 distinct LC sequences, primarily of the lambda (λ) isotype (11), have been identified in AL amyloid deposits, reflecting the significant protein heterogeneity associated with AL proteotoxicity (12). Amyloidogenic LCs generally contain an energetically destabilized variable domain that facilitates LC aggregation (2).

The amyloidogenic LC plasma concentration is determined by the extent of LC secretion from plasma cells and the rate of LC turnover in the serum. Secretion efficiency is largely dictated by the balance between folding vs. degradation, often referred to as "quality control," in the endoplasmic reticulum (ER) (13). ER quality control is determined by the activity of the ER protein homeostasis (proteostasis) network comprising the protein folding, secretion, and degradation pathways (14–19). These pathways primarily function to prevent the secretion of destabilized, misfolding-prone proteins into the extracellular space (14–19).

Plasma cells have an evolutionarily enhanced ER and secretory pathway, enabling the proper folding and secretion of >1,000 IgGs per second (20, 21). Plasma cells normally secrete LC as IgGs [assemblies of two LCs and two heavy chains (HCs)], or as free LCs. However, in AL patients, LCs are predominantly secreted independent of HCs, sometimes as monomers, but generally as disulfide-linked homodimers called Bence–Jones proteins—the common precursor for LC aggregation (22, 23). Furthermore, LC ER quality

Significance

Light-chain amyloidosis (AL) is a devastating human disease involving the clonal expansion of a plasma cell and the secretion of destabilized, amyloidogenic immunoglobulin light chains (LCs). Secreted amyloidogenic LCs aggregate extracellularly, leading to proteotoxicity on distal tissues. Available therapeutic strategies to treat AL specifically target the cancerous plasma cell population. While this approach is effective in ∼70% of patients, patients who present with substantial LC-related organ proteotoxicity are generally too sick to tolerate standard chemotherapeutics. Here, we show that stress-independent activation of unfolded protein response-associated transcription factors selectively reduces secretion of amyloidogenic LCs and decreases extracellular soluble LC aggregates associated with proteotoxicity in AL. These results identify a promising therapeutic strategy to treat AL patients unserved by current treatments.

Author contributions: C.B.C., L.M.R., L.P., J.W.K., and R.L.W. designed research; C.B.C., L.M.R., L.P., G.J.M., and R.L.W. performed research; J.D.H. contributed new reagents/analytic tools; C.B.C., L.M.R., L.P., G.J.M., and R.L.W. analyzed data; C.B.C., L.M.R., L.P., G.J.M., J.W.K., and R.L.W. wrote the paper; and J.W.K. and R.L.W. provided oversight.

The authors declare no conflict of interest.

This article is a PNAS Direct Submission.

[1]C.B.C. and L.M.R. contributed equally to this work.

[2]Present address: Departments of Ophthalmology and Pharmacology, University of Texas Southwestern Medical Center, Dallas, TX 75390.

[3]To whom correspondence may be addressed. Email: wiseman@scripps.edu or jkelly@scripps.edu.

This article contains supporting information online at www.pnas.org/lookup/suppl/doi:10.1073/pnas.1406050111/-/DCSupplemental.

control is compromised in AL, allowing the efficient secretion of destabilized, amyloidogenic LC sequences that can aggregate extracellularly into proteotoxic soluble oligomers and amyloid fibrils.

Herein, we sought to identify signaling pathways that can be activated to reduce the secretion of destabilized, amyloidogenic LCs, thus reducing the extracellular LC concentration available for pathologic, concentration-dependent aggregation. Using a small-molecule screening approach, we identified that unfolded protein response (UPR) (24, 25) activation selectively reduces the secretion of a destabilized, amyloidogenic LC but not a more stable, nonamyloidogenic LC sequence. The UPR transcriptionally upregulates ER quality control in response to ER stress, primarily through the transcription factors XBP1s and/or ATF6, comprising the adaptive UPR (25). Here, we show that stress-independent activation of XBP1s and especially ATF6 is sufficient to reduce amyloidogenic LC secretion and attenuate LC aggregation. Collectively, our results demonstrate that enhancing ER quality control via adaptive UPR activation represents a therapeutic strategy to ameliorate LC aggregation-associated proteotoxicity.

Results

Screening Reveals That UPR Activation Reduces Amyloidogenic LC Secretion. We developed a secretion reporter for LC by fusing the well-characterized AL-causing Vλ6 LC containing both constant and variable LC domains (named ALLC) (26) to an enhanced *Gaussia princeps* luciferase (GLuc) reporter, ALLC-GLuc (Fig. 1*A*) (27, 28). We used a similar GLuc fusion approach to quantify secretion of other proteins in a cell-based high-throughput screening (HTS) format (29). The secretion of ALLC-GLuc from HEK293-TRex cells was observable by immunoblotting and luminescence (Fig. S1 *A* and *B*). ALLC secretion decreased upon inhibition of protein biosynthesis using cycloheximide (CHX) or after inhibition of global protein secretion using brefeldin A (Fig. S1*C*), as did the secretion of GLuc, used as a control. ALLC-GLuc or GLuc was then stably incorporated into retinal pigment epithelium (ARPE-19) cells, as we previously optimized these professional secretory cells for HTS of GLuc fusion proteins such as ALLC-GLuc (29). The ALLC-GLuc secretion assay was miniaturized to a 384-well plate format, affording an HTS z-score (30) of 0.65 using cycloxheximide as a control.

To identify biologic pathways that selectively reduce secretion of ALLC-GLuc, we screened the Library of Pharmacologically Active Compounds (LOPAC, Sigma Aldrich) in ARPE-19 cells secreting ALLC-GLuc or GLuc. The LOPAC was chosen because it is moderately sized (1,280 compounds), consists of compounds from major drug categories, and the biological targets for many small molecule components are known. We identified 15 molecules that significantly reduced ALLC-GLuc secretion (>25% reduction vs. vehicle control, 24-h treatment), while not affecting GLuc secretion (Fig. 1*B*, section shaded blue). Molecules that disrupted both ALLC-GLuc and GLuc secretion were not pursued further, as these likely reduce protein synthesis and/or disrupt global cell secretion (e.g., CHX and brefeldin A in Fig. S1*C*). Interestingly, the UPR activators thapsigargin (Tg), an inhibitor of sarco/endoplasmic reticulum Ca^{2+}-ATPase (31), and ellipticene (32) selectively reduced ALLC secretion relative to GLuc (Fig. 1*B*), suggesting that activation of the UPR could selectively influence LC secretion. The inability of a 24-h treatment with Tg to influence GLuc secretion is consistent with previous results (27).

To further examine the relationship between UPR activation and the reduction in ALLC-GLuc secretion, we performed an additional screen using HEK293T-Rex cells stably expressing firefly luciferase under the control of the ER stress-responsive element (ERSE) promoter (ERSE-FLuc, Fig. 1*A*) (33). We found that 7 out of 15 molecules that selectively reduce ALLC-GLuc secretion by >25% also activated the ERSE-FLuc reporter >1.5 fold (Fig. 1*C*, blue), indicating that molecules that reduce ALLC-GLuc secretion are enriched for UPR activators.

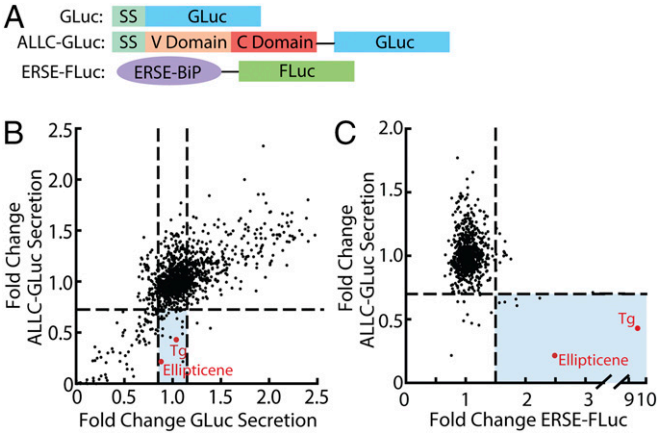

Fig. 1. ALLC-GLuc reporter screening identifies UPR modulators able to reduce secretion of amyloidogenic LC. (*A*) Schematic of GLuc, ALLC-GLuc, and ERSE-FLuc reporter constructs used in stable ARPE19 or HEK293T-Rex cell lines. ERSE-FLuc transcriptional reporter includes the ERSE-containing portion of the BiP promoter upstream of the firefly luciferase (FLuc) gene. SS, signal sequence. (*B*) Plot of LOPAC screening data comparing ALLC-GLuc secretion vs. GLuc secretion. ARPE-19 cells stably expressing ALLC-GLuc or GLuc alone were treated with compound (10 μM) for 24 h. Shaded blue section indicates compounds that reduce ALLC-GLuc secretion (>25%) and do not affect GLuc secretion (<±15% from DMSO control). (*C*) Plot of LOPAC screening results comparing ALLC-GLuc secretion (ARPE-19 cells, 24-h treatment) vs. UPR activation (ERSE-FLuc expressing HEK293T-Rex cells, 18-h treatment). Compounds falling below the horizontal line reduce ALLC-GLuc secretion by 25%. Compounds falling to the right of the vertical line increase ERSE-FLuc expression >1.5-fold relative to DMSO control. Compounds depicted in red are known activators of the UPR.

Thapsigargin Selectively Reduces ALLC Secretion. To further understand the effect of ER stress-associated UPR activation on LC secretion, we used [^{35}S]-metabolic labeling to measure the secretion of amyloidogenic ALLC fused to an N-terminal FLAG tag (^{FT}ALLC, Fig. 2*A*). We preincubated cells in the absence or presence of Tg for 15 h to promote UPR-dependent remodeling of the ER proteostasis network before [^{35}S]-metabolic labeling (Fig. 2*A*). ^{FT}ALLC was immunopurified from media and cell lysates at specific timepoints during a 4-h chase in non-radioactive media. These experiments show that Tg pretreatment reduces ^{FT}ALLC secretion by >40% (Fig. 2*B*). Importantly, because our Tg treatments do not drastically influence cell viability (Fig. S2 *A* and *B*), the Tg-dependent reduction in ALLC secretion cannot be attributed to cell toxicity. Furthermore the Tg-dependent reduction in ALLC secretion is also observed in cells treated with the protein kinase R-like ER kinase (PERK) inhibitor GSK2606414 (34), demonstrating that the reduced secretion does not result from PERK-dependent translational attenuation (Fig. S2*C*).

No accumulation of ^{FT}ALLC was observed in cell pellets following ER stress caused by Tg treatment (Fig. 2*C*), indicating that ALLC does not accumulate as intracellular aggregates. Reduced ^{FT}ALLC secretion was associated with a decrease in total [^{35}S]-labeled ^{FT}ALLC (media + lysate) (Fig. 2*D*), suggesting that Tg-associated ER stress increases ^{FT}ALLC degradation. Similar results were obtained with an untagged ALLC, confirming that the FLAG tag does not significantly influence ALLC secretion and/or degradation (Fig. S2 *D* and *E*). This Tg-dependent loss in total ^{FT}ALLC cannot be reversed using proteasome inhibitors (bortezomib or MG132) or the p97 inhibitor eeyarestatin I [a potent inhibitor of ER-associated degradation (ERAD) (35)],

BIOCHEMISTRY

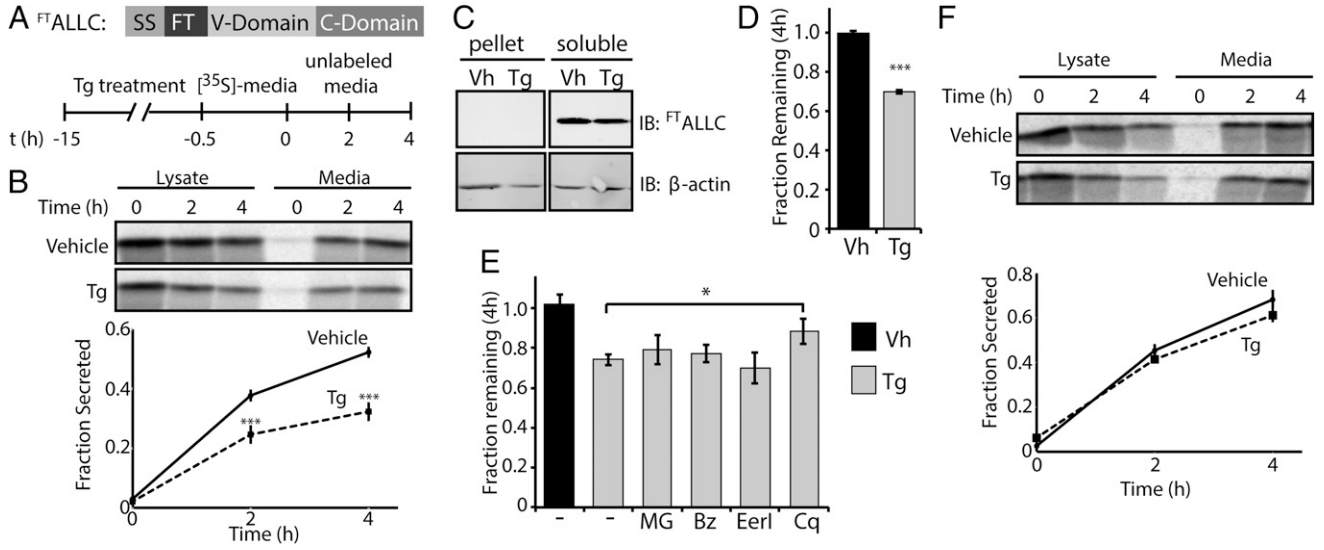

Fig. 2. Thapsigargin selectively reduces the secretion of amyloidogenic LC and induces its degradation. (*A*) Schematic of the ^{FT}ALLC construct used in pulse-chase experiments and the metabolic labeling protocol used. [^{35}S]-labeled ^{FT}ALLC was immunopurified from media and lysates collected from transfected HEK293T-Rex cells following a 15-h treatment with thapsigargin (Tg, 500 nM). (*B*) Representative autoradiogram and quantification of [^{35}S]-labeled ^{FT}ALLC in pulse-chase experiment described in *A*. Fraction secreted was calculated as described in *Materials and Methods* (18) ($n \geq 3$). (*C*) Immunoblots measuring soluble and insoluble (pellet) levels of ^{FT}ALLC after 15-h pretreatment with Tg. (*D*) Graph depicting total [^{35}S]-labeled ^{FT}ALLC (combined media and lysate protein levels as in *B*) remaining at 4 h in HEK293T-Rex cells following a 15-h pretreatment with 500 nM Tg ($n \geq 3$). The fraction remaining was calculated as described in *Materials and Methods* (18). (*E*) Graph depicting the fraction recovery of total [^{35}S]- labeled ^{FT}ALLC at 4 h in HEK293T-Rex cells incubated in the presence of thapsigargin (Tg; 500 nM, 15 h) and the proteasome inhibitors bortezomib (Bz; 20 μM) or MG132 (MG; 20 μM), the ERAD inhibitor eeyarestatin I (EerI; 20 μM), or the autophagy inhibitor chloroquine (Cq; 100 μM). Inhibitors were incubated for 4 h before [^{35}S] metabolic labeling and included throughout the labeling protocol shown in *A*. Fraction remaining was calculated as in *D* ($n \geq 2$). (*F*) Representative autoradiogram and quantification of [^{35}S]-labeled ^{FT}JTO immunopurified from media and lysates collected from transfected HEK293T-Rex cells following the same protocol and quantification as in *A* and *B* ($n \geq 3$). *$P < 0.05$; ***$P < 0.005$. All error bars represent the SEM from biological replicates.

indicating that ^{FT}ALLC is degraded following ER stress, at least in part through an ERAD-independent mechanism (Fig. 2*E*) (36). In contrast, the autophagy inhibitor chloroquine stabilized ALLC against Tg-induced degradation, indicating that Tg increases the autophagic degradation of ALLC (Fig. 2*E*).

Destabilized proteins are sensitive to UPR-dependent remodeling of the ER proteostasis network, whereas stable variants are generally less sensitive to this remodeling (37). Thus, we evaluated whether Tg-dependent reductions in LC secretion are also observed for a nonamyloidogenic, full-length Vλ6 LC, ^{FT}JTO (38). Tg pretreatment did not reduce the secretion of [^{35}S]-labeled, nonamyloidogenic ^{FT}JTO (Fig. 2*F*), indicating that Tg-dependent UPR activation selectively reduces the secretion of an amyloidogenic, but not a nonamyloidogenic LC.

LC amyloidogenicity is highly correlated with LC stability (38, 39). Thus, we compared the in vitro relative stability of recombinant ALLC and JTO. Circular dichroism and tryptophan fluorescence measurements confirmed that the recombinant proteins have a folded, native β-sheet-rich Ig structure (Fig. S3 *A* and *B*). The relative stability of the ALLC and JTO LCs were compared by urea denaturation and monitored by tryptophan fluorescence (Fig. S3*C*). Although the ALLC unfolding transition is not completely reversible (Fig. S3*A*, black curve), the urea midpoint values for the denaturation curves (ALLC 1.8 M, JTO 2.6 M) indicate that ALLC is less stable than JTO (Fig. S3*C*). This suggests that the selective decrease in ALLC secretion afforded by Tg could be attributed to the inherent instability of the ALLC protein.

XBP1s and/or ATF6 Activation Reduces the Secretion of Destabilized ALLC. Previous work has indicated that remodeling of ER proteostasis pathways selectively influences the secretion of destabilized protein variants relative to more stable protein variants (13, 40, 41). Thus, Tg-dependent UPR activation could selectively decrease the secretion of destabilized ALLC through the transcriptional remodeling of the ER proteostasis network. To differentiate between the potential effects of Tg-induced ER stress and UPR-dependent remodeling of ER proteostasis pathways on ALLC secretion, we used a HEK293T-Rex-derived cell line that expresses both a ligand-regulatable ATF6 transcription factor [DHFR-ATF6; activated by the addition of the small molecule pharmacologic chaperone trimethoprim (TMP)] and a doxycycline (Dox)-inducible XBP1s transcription factor (cells referred to as HEK293^{DAX}) (40). In these cells, the ATF6 or XBP1s transcriptional programs can be orthogonally controlled in the absence of ER stress, which enables analysis of the functional consequences of arm-selective UPR activation independently, or in combination (Fig. S4*A*) (40).

We treated HEK293^{DAX} cells expressing ^{FT}ALLC with Dox, TMP, or Tg and quantified the ^{FT}ALLC levels in conditioned media by ELISA (Fig. 3*A*). Stress-independent activation of XBP1s or ATF6 reduced extracellular ^{FT}ALLC levels to 68% and 48% of vehicle levels, respectively. Tg treatment lowered ^{FT}ALLC levels to 34%. Reduced ^{FT}ALLC secretion induced by XBP1s or ATF6 activation was dependent on transcription factor activity, as no reduction in ^{FT}ALLC secretion was observed in TMP- or Dox-treated HEK293^{DYG} cells—a control cell line stably expressing DHFR-YFP and Dox-inducible GFP (Fig. S4*B*) (40).

To probe the basis for the XBP1s- or ATF6-mediated reduction in ALLC secretion, we used [^{35}S]-metabolic labeling (Fig. 3 *B*–*E*). XBP1s, ATF6, or combinatorial activation lowered the relative secreted fraction of labeled ALLC by ∼40% following a 4-h chase (Fig. 3 *B* and *C*). In contrast, stress-independent activation of XBP1s and/or ATF6 did not affect the secretion of the nonamyloidogenic ^{FT}JTO (Fig. S4*C*). Notably, XBP1s- and ATF6-dependent reductions in ALLC secretion proceed through distinct mechanisms. XBP1s activation resulted in a 25% decrease in total [^{35}S]-labeled ^{FT}ALLC (Fig. 3*D*), as observed for Tg-treatment (Fig. 2*D*). This XBP1s-dependent decrease in total soluble ALLC was not

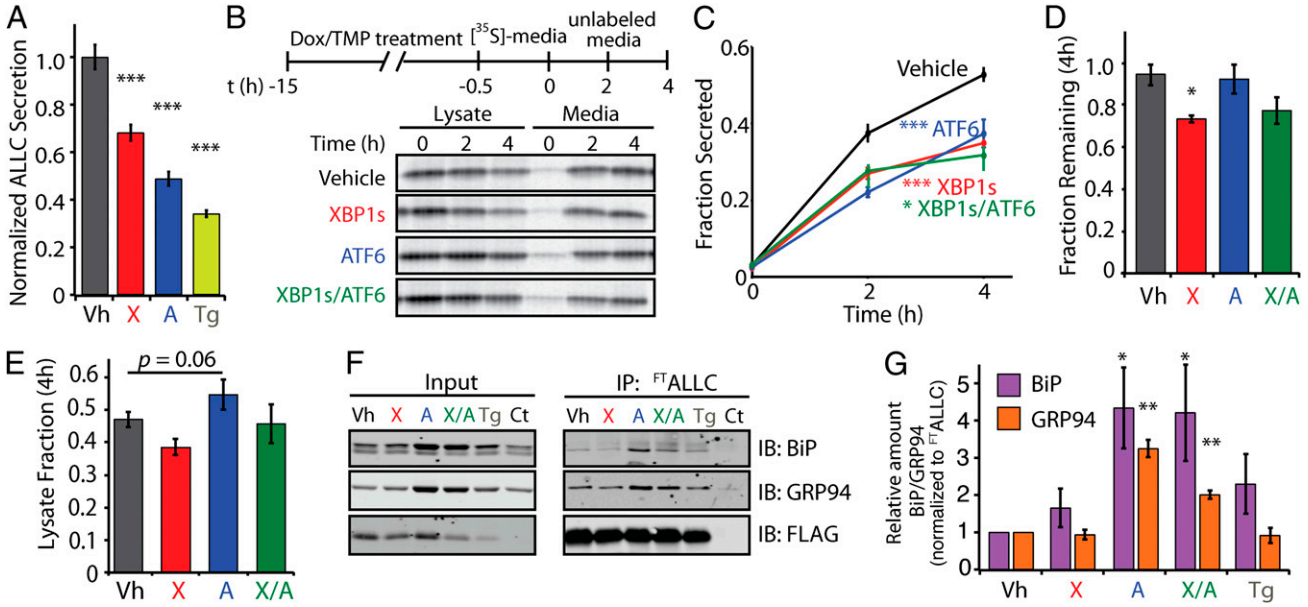

Fig. 3. Stress-independent activation of XBP1s and/or ATF6 decreases the secretion of amyloidogenic LC. (*A*) ALLC levels determined by ELISA in conditioned media from HEK293^{DAX} cells (40) expressing ^{FT}ALLC following a 15-h preactivation of XBP1s (X; Dox, 1 μg/mL) or ATF6 (A; TMP, 10 μM) or by thapsigargin-induced stress (Tg, 500 nM). ALLC secretion levels were normalized to vehicle (Vh; DMSO) conditions ($n = 3$). (*B*) Representative autoradiogram of [^{35}S]-labeled ^{FT}ALLC immunopurified from media and lysates collected from transfected HEK293T-Rex cells following a 15-h preactivation of XBP1s (X; Dox, 1 μg/mL), ATF6 (A; TMP, 10 μM), or both (X/A). The metabolic labeling protocol used is shown. (*C*) Quantification of fraction secreted from autoradiograms as shown in *B* ($n \geq 3$). (*D*) Graph depicting the total [^{35}S]-labeled ^{FT}ALLC remaining at 4 h in lysate and media following a 15-h preactivation of XBP1s, ATF6, or both in HEK293^{DAX} ($n \geq 3$). (*E*) Graph depicting the total intracellular [^{35}S]-labeled ^{FT}ALLC in lysates at 4 h in HEK293^{DAX} cells following a 15-h preactivation of XBP1s, ATF6, or both ($n \geq 3$). The lysate fraction was calculated by dividing the lysate [^{35}S]-labeled FTALLC signal at 4 h by the total [^{35}S]-labeled ^{FT}ALLC at t = 0. (*F*) Immunoblot showing the recovery of the ER chaperones BiP and GRP94 in FLAG immunopurifications from cross-linked HEK293^{DAX} cells expressing ^{FT}ALLC following 15-h pretreatment with thapsigargin (Tg), XBP1s (X), ATF6 (A), or XBP1s and ATF6 (X/A), as in *B*. HEK293^{DAX} cells expressing untagged ALLC is shown as a control (Ct). (*G*) Quantification of *F* achieved by comparing the signal under various conditions to vehicle, and by normalizing to the recovered ^{FT}ALLC. *$P < 0.05$; **$P < 0.01$; ***$P < 0.005$. All error bars represent the SEM from biological replicates.

a result of intracellular accumulation of ^{FT}ALLC in the cell pellet (Fig. S4*D*), implying the loss of ^{FT}ALLC is due to degradation and not intracellular aggregation. ATF6 activation, in contrast, did not decrease total ALLC recovery in our [^{35}S] metabolic labeling experiments (Fig. 3*D*) but instead resulted in an increase in intracellular [^{35}S]-labeled ^{FT}ALLC (Fig. 3*E*). Coactivation of XBP1s and ATF6 decreases ^{FT}ALLC recovery to that observed for XBP1s activation. Similar results were observed with untagged ALLC (Fig. S5).

Altered processing of ALLC in the ER after XBP1s and/or ATF6 activation likely reflects distinct interactions between ALLC and ER proteostasis network components differentially induced by these transcriptional programs. We used an in situ cross-linking and immunopurification approach to sensitively measure the intracellular associations between ALLC and ER chaperones such as BiP (GRP78) and GRP94 (Fig. S6*A*)—two ER chaperones known to interact with LC (42, 43). As predicted, ATF6 activation, but not XBP1s activation, resulted in a significant increase in the association between ALLC and the ATF6-regulated ER chaperones BiP and GRP94 (Fig. 3 *F* and *G*), reflecting the increased levels of these two ER chaperones afforded by ATF6 activation (40). The increased association between ALLC and these ER proteostasis factors provides a mechanism to explain the ATF6-induced intracellular retention of destabilized, aggregation-prone ALLC in the ER lumen. ATF6 activation also increased interactions between ^{FT}JTO and BiP and GRP94 (Fig. S6*B*), albeit to a lesser extent than that observed for ALLC (Fig. 3 *F* and *G*).

XBP1s and/or ATF6 Decreases Extracellular Aggregation of Secreted ALLC. Lowering the secretion of an amyloidogenic LC should directly ameliorate AL organ proteotoxicity by reducing the extracellular concentration and therefore the extracellular aggregation of amyloidogenic LCs. To scrutinize this hypothesis, we examined the concentration-dependent aggregation of recombinant ALLC by monitoring turbidity of samples heated to 44 °C (Fig. 4 *A* and *B*). Reducing the concentration of ALLC significantly reduced the extent (Fig. 4*A*) and rate of aggregation (Fig. 4*B*), demonstrating that recombinant ALLC aggregates through a concentration-dependent mechanism.

Because XBP1s and/or ATF6 activation decreases the secretion of amyloidogenic LC, we reasoned that the stress-independent activation of these transcriptional programs would similarly decrease extracellular ALLC aggregation. Heating the conditioned media of cells expressing ^{FT}ALLC to 55 °C for 0–24 h produced large soluble aggregates that increase with time, as discerned by blue native polyacrylamide gel electrophoresis (BN-PAGE) (Fig. S7*A*) and gel filtration chromatography (Fig. S7*B*). Reducing the extracellular concentration of ^{FT}ALLC in conditioned media by dilution with media conditioned on GFP-transfected cells shows that cell-secreted ALLC aggregation is concentration dependent (Fig. 4*C*), where a 1:1 [50% (vol/vol)] dilution of ALLC conditioned media nearly eliminates ALLC aggregates.

We next evaluated whether stress-independent XBP1s and/or ATF6 activation similarly attenuates ALLC aggregation. We collected conditioned media from ^{FT}ALLC-expressing HEK293^{DAX} cells following XBP1s and/or ATF6 activation and measured ALLC aggregation using BN-PAGE. ATF6 activation resulted in a 73% loss of soluble ^{FT}ALLC aggregates (55 °C, 8 h incubation; Fig. 4 *D* and *E*), whereas XBP1s activation resulted in a 20% loss, and activating both XBP1s and ATF6 reduced aggregate formation by 60% (Fig. 4 *D* and *E*). As expected, the reduction in ALLC aggregation corresponds with a decrease in total extracellular ALLC (Fig. 4 *D* and *E*). Interestingly, the reduction in ALLC

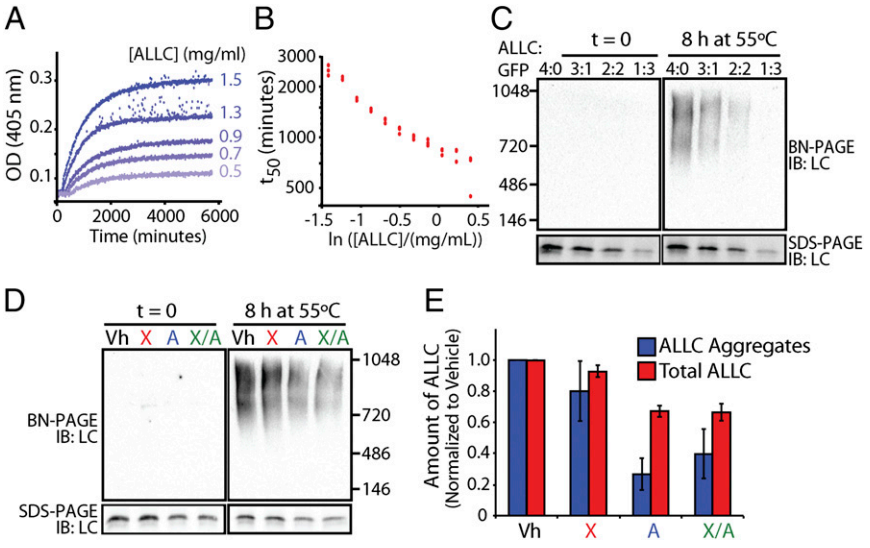

Fig. 4. Stress-independent activation of XBP1s and especially ATF6 reduces aggregation of cell-secreted ALLC. (*A*) Timecourses of recombinant ALLC aggregation at the indicated concentrations. Samples were incubated at 44 °C for the indicated time, and aggregation was measured by turbidity at 405 nm. (*B*) Plot of the t_{50} of recombinant ALLC aggregation at the indicated concentration from data as shown in *A*; $n = 3$ replicates are shown. (*C*) Immunoblots for BN-PAGE and SDS-PAGE of media conditioned on HEK293^{DAX} cells expressing ^{FT}ALLC for 24 h. The media was diluted with media conditioned on GFP-expressing cells, as indicated, and incubated at 55 °C for 8 h. (*D*) Representative immunoblots for BN-PAGE and SDS-PAGE of media conditioned on HEK293^{DAX} cells following a 16-h preactivation of XBP1s (*X*), ATF6 (A), or XBP1s and ATF6 (*X*/A), as in Fig. 3*B*. ^{FT}ALLC aggregation was induced by incubating the media for 8 h at 55 °C. (*E*) Graph depicting the quantification of soluble aggregates and total ALLC from BN-PAGE and SDS-PAGE immunoblots, as shown in *D*, normalized to vehicle. Error bars represent SEM from biological replicates ($n = 3$).

aggregation was more pronounced than expected from just the reduction in total extracellular ALLC, suggesting that XBP1s and/or ATF6 activation could also influence ALLC aggregation through other mechanisms. Importantly, we do not observe significant associations between ALLC and the ER chaperones BiP and GRP94 in conditioned media, indicating that the reduction in extracellular ALLC aggregation cannot be attributed to increased association with these ER chaperones secreted from cells (Fig. S8*A*). ALLC secretion and aggregation was not sensitive to treatment with Dox, TMP, or both in the control HEK293^{DYG} cells (Fig. S8*B*), demonstrating that the reduced aggregation of ALLC observed in HEK293^{DAX} requires XBP1s and/or ATF6 transcriptional activity.

Discussion

We show that stress-independent activation of one or both of the adaptive UPR-associated transcription factors XBP1s or especially ATF6 reduces the secretion and extracellular concentration of amyloidogenic ALLC, reducing soluble ALLC aggregate levels. This strategy has the potential to be clinically meaningful, as a >50% reduction in the amount of circulating amyloidogenic LC mediated by chemotherapeutic methods correlates with a substantial survival benefit (44). Lowering the amount of amyloidogenic LC secreted from plasma cells into the blood by UPR activation should be useful in patients with significant cardiac and/or renal involvement. This approach, with time, should dramatically reduce amyloidogenic LC oligomer levels and thus proteotoxicity, enabling the patient to tolerate established chemotherapy regimens. Arm-selective UPR activation could also be used in combination with chemotherapy approaches to further reduce the amount of circulating LC and organ proteotoxicity. Lastly, the approach could potentially be useful in cases of AL recurrence, decreasing the amyloidogenic LC secretion and organ proteotoxicity in chemotherapy-resistant AL patients.

Partitioning of amyloidogenic LCs between folding and trafficking vs. degradation pathways is determined by the interactions between the destabilized LC and ER proteostasis network components. The stoichiometry of the components of the ER proteostasis network is regulated by the activated signaling arms of the UPR (40). This in turn determines the specific ER proteostasis factors that interact with amyloidogenic LC and, thus, dictates the partitioning of LC between retention, secretion, or degradation in the ER lumen. The degradation of ^{FT}ALLC upon XBP1s activation accounts for most of the observed reduction in secretion. In contrast, ATF6 activation does not induce ALLC degradation in HEK293^{DAX} but instead leads to intracellular retention of ALLC, consistent with the increased interactions between ALLC and the ER chaperones BiP and GRP94. In AL-patient plasma cells, the retention of an amyloidogenic LC could sensitize the cells to death by subsequent chemotherapy strategies, or by itself be cytotoxic. Alternatively, degradation could eventually occur with repeated but periodic ATF6 activation, although this potential mechanism needs to be further explored. Increasing ER quality control by arm-selective UPR activation appears to be a general approach to reduce the secretion of destabilized, aggregation-prone proteins (37). Activation of ATF6 selectively reduces the secretion of destabilized, amyloidogenic transthyretin mutants from hepatocytes and can reduce intracellular accumulation of mutant rhodopsin, while not affecting secretion of the wild-type proteins (40, 41), providing strong support for this hypothesis.

Based on the results described above, we are now seeking small molecules that activate the ATF6 and/or XBP1s arms of the UPR. These small molecules would transcriptionally remodel the ER proteostasis network in plasma cells, reducing the secretion of energetically destabilized LCs irrespective of their primary structure, obviating the need for sequence- and conformation-specific AL drug design challenged by the significant sequence heterogeneity associated with LC proteotoxicity in AL. Furthermore, based on other reports demonstrating the capacity of XBP1s and/or ATF6 activation to influence aberrant ER quality control linked to disease-associated proteotoxicity (40, 41), establishing small molecules that increase ER quality control is expected to have significant potential for the treatment of additional protein aggregation diseases.

Materials and Methods

Plasmids, Cell Culture, HTS, and Recombinant Protein Production. Detailed protocols can be found in *SI Materials and Methods*.

Pulse-Chase Experiments. HEK293^{DAX} or HEK293T-Rex cells plated on poly-D-lysine coated plates were metabolically labeled in DMEM -Cys/-Met (CellGro) supplemented with glutamine, penicillin/streptomycin, 10% dialyzed FBS, and [^{35}S]-Translabel (MP Biomedical) for 30 min. Cells were washed with complete media and incubated in DMEM for the indicated times and harvested at the indicated times. In the case of added inhibitors, cells were pretreated for 4 h at the indicated concentrations, and inhibitors were added to the pulse and chase media. Lysates were prepared in radioimmunoprecipitation assay buffer plus protease inhibitor mixture (Roche) with 10 mM $CaCl_2$. Proteins were immunopurified using anti-FLAG M1 agarose beads (Sigma). Protein was eluted by boiling in Laemmli buffer + 100 mM DTT, and samples were separated by SDS-PAGE. The gels were dried, exposed to phosphorimager plates (GE Healthcare),

and imaged with a Typhoon imager. Band intensities were quantified in ImageQuant. Fraction secreted was calculated using the equation: fraction secreted = [extracellular [^{35}S]-LC signal at t = t/(extracellular [^{35}S]-LC signal at t = 0 + intracellular [^{35}S]-LC signal at t = 0)]. Fraction remaining was calculated using the equation: [(extracellular [^{35}S]-LC signal at t = t + intracellular [^{35}S]-LC signal at t = t)/(extracellular [^{35}S]-LC signal at t = 0 + intracellular [^{35}S]-LC signal at t = 0)].

Conditioned Media Aggregation and Blue Native PAGE. HEK293^{DAX} cells expressing LC or GFP control were treated with vehicle, doxycycline (Dox), trimethoprim (TMP), or the combination for 16 h. The medium was removed, centrifuged at 200 × *g* to remove cell debris, transferred to a new tube, and protease inhibitor mixture (Roche) added. The medium was incubated at 55 °C with aliquots removed at the indicated timepoints.

Conditioned medium was added to blue native PAGE loading dye (10% glycerol, 0.5% Coomassie G-250) and then loaded onto 3–12% Bis-Tris gradient gels (Invitrogen). The cathode buffer contained 50 mM Tricene and 15 mM Bis-Tris, pH 7.0 with 0.02% Coomassie G-250. The anode buffer contained 50 mM Bis-Tris pH 7.0. The gels were transferred onto PVDF membranes, and LC was detected by polyclonal anti-human lambda LC (Bethyl Laboratories), followed by HRP-conjugated secondary antibodies. The blots were imaged using a chemiluminescence substrate (Luminata Forte Western Luminescence Substrate, Millipore) and imaged by film or with a Bio-Rad scanner.

ACKNOWLEDGMENTS. We thank William Balch for helpful discussions. We thank Arlene and Arnold Goldstein, the National Institutes of Health (NIH) (AG046495, DK075295, and NS079882), the Ellison Medical Foundation, the Skaggs Institute for Chemical Biology, the Lita Annenberg Hazen Foundation, and the Scripps Research Institute for financial support. C.B.C. was supported by NIH (F32 AG042259).

1. Cohen AD, Comenzo RL (2010) Systemic light-chain amyloidosis: Advances in diagnosis, prognosis, and therapy. *Hematology (Am Soc Hematol Educ Program)* 2010: 287–294.
2. Buxbaum JN, Linke RP (2012) A molecular history of the amyloidoses. *J Mol Biol* 421(2-3):142–159.
3. Jones NF, Hilton PJ, Tighe JR, Hobbs JR (1972) Treatment of "primary" renal amyloidosis with melphalan. *Lancet* 2(7778):616–619.
4. Jaccard A, et al.; Myélome Autogreffe (MAG) and Intergroupe Francophone du Myélome (IFM) Intergroup (2007) High-dose melphalan versus melphalan plus dexamethasone for AL amyloidosis. *N Engl J Med* 357(11):1083–1093.
5. Kastritis E, et al. (2010) Bortezomib with or without dexamethasone in primary systemic (light chain) amyloidosis. *J Clin Oncol* 28(6):1031–1037.
6. Venner CP, et al. (2012) Cyclophosphamide, bortezomib, and dexamethasone therapy in AL amyloidosis is associated with high clonal response rates and prolonged progression-free survival. *Blood* 119(19):4387–4390.
7. Reece DE, et al. (2011) Efficacy and safety of once-weekly and twice-weekly bortezomib in patients with relapsed systemic AL amyloidosis: Results of a phase 1/2 study. *Blood* 118(4):865–873.
8. Comenzo RL, Gertz MA (2002) Autologous stem cell transplantation for primary systemic amyloidosis. *Blood* 99(12):4276–4282.
9. Palladini G, et al. (2004) Association of melphalan and high-dose dexamethasone is effective and well tolerated in patients with AL (primary) amyloidosis who are ineligible for stem cell transplantation. *Blood* 103(8):2936–2938.
10. Merlini G, Seldin DC, Gertz MA (2011) Amyloidosis: Pathogenesis and new therapeutic options. *J Clin Oncol* 29(14):1924–1933.
11. Solomon A, Weiss DT, Pepys MB (1992) Induction in mice of human light-chain-associated amyloidosis. *Am J Pathol* 140(3):629–637.
12. Bodi K, et al. (2009) AL-Base: A visual platform analysis tool for the study of amyloidogenic immunoglobulin light chain sequences. *Amyloid* 16(1):1–8.
13. Wiseman RL, Powers ET, Buxbaum JN, Kelly JW, Balch WE (2007) An adaptable standard for protein export from the endoplasmic reticulum. *Cell* 131(4):809–821.
14. Balch WE, Morimoto RI, Dillin A, Kelly JW (2008) Adapting proteostasis for disease intervention. *Science* 319(5865):916–919.
15. Smith MH, Ploegh HL, Weissman JS (2011) Road to ruin: Targeting proteins for degradation in the endoplasmic reticulum. *Science* 334(6059):1086–1090.
16. Lindquist SL, Kelly JW (2011) Chemical and biological approaches for adapting proteostasis to ameliorate protein misfolding and aggregation diseases: Progress and prognosis. *Cold Spring Harb Perspect Biol* 3(12):a004507.
17. Hartl FU, Bracher A, Hayer-Hartl M (2011) Molecular chaperones in protein folding and proteostasis. *Nature* 475(7356):324–332.
18. Sekijima Y, et al. (2005) The biological and chemical basis for tissue-selective amyloid disease. *Cell* 121(1):73–85.
19. Powers ET, Morimoto RI, Dillin A, Kelly JW, Balch WE (2009) Biological and chemical approaches to diseases of proteostasis deficiency. *Annu Rev Biochem* 78:959–991.
20. Cenci S, Sitia R (2007) Managing and exploiting stress in the antibody factory. *FEBS Lett* 581(19):3652–3657.
21. Ma Y, Hendershot LM (2003) The stressful road to antibody secretion. *Nat Immunol* 4(4):310–311.
22. Williamson AR, Adkonas BA (1968) Time course of labeling of light and heavy chains of immunoglobulin G and the turnover of the free light-chain intermediates. *Arch Biochem Biophys* 125(2):401–409.
23. Zolla S, Buxbaum J, Franklin EC, Scharff MD (1970) Synthesis and assembly of immunoglobulins by malignant human plasmacytes. I. Myelomas producing gamma-chains and light chains. *J Exp Med* 132(1):148–162.
24. Walter P, Ron D (2011) The unfolded protein response: From stress pathway to homeostatic regulation. *Science* 334(6059):1081–1086.
25. Wang S, Kaufman RJ (2012) The impact of the unfolded protein response on human disease. *J Cell Biol* 197(7):857–867.
26. Arendt BK, et al. (2008) Biologic and genetic characterization of the novel amyloidogenic lambda light chain-secreting human cell lines, ALMC-1 and ALMC-2. *Blood* 112(5):1931–1941.
27. Badr CE, Hewett JW, Breakefield XO, Tannous BA (2007) A highly sensitive assay for monitoring the secretory pathway and ER stress. *PLoS ONE* 2(6):e571.
28. Hulleman JD, Balch WE, Kelly JW (2012) Translational attenuation differentially alters the fate of disease-associated fibulin proteins. *FASEB J* 26(11):4548–4560.
29. Hulleman JD, Brown SJ, Rosen H, Kelly JW (2013) A high-throughput cell-based Gaussia luciferase reporter assay for identifying modulators of fibulin-3 secretion. *J Biomol Screen* 18(6):647–658.
30. Zhang JH, Chung TD, Oldenburg KR (1999) A simple statistical parameter for use in evaluation and validation of high throughput screening assays. *J Biomol Screen* 4(2): 67–73.
31. Li WW, Alexandre S, Cao X, Lee AS (1993) Transactivation of the grp78 promoter by Ca2+ depletion. A comparative analysis with A23187 and the endoplasmic reticulum Ca(2+)-ATPase inhibitor thapsigargin. *J Biol Chem* 268(16):12003–12009.
32. Hägg M, et al. (2004) Induction of endoplasmic reticulum stress by ellipticine plant alkaloids. *Mol Cancer Ther* 3(4):489–497.
33. Hiramatsu N, Joseph VT, Lin JH (2011) Monitoring and manipulating mammalian unfolded protein response. *Methods Enzymol* 491:183–198.
34. Axten JM, et al. (2012) Discovery of 7-methyl-5-(1-[3-(trifluoromethyl)phenyl]acetyl-2,3-dihydro-1H-indol-5-yl)-7H-pyrrolo[2,3-d]pyrimidin-4-amine (GSK2606414), a potent and selective first-in-class inhibitor of protein kinase R (PKR)-like endoplasmic reticulum kinase (PERK). *J Med Chem* 55(16):7193–7207.
35. Wang Q, Li L, Ye Y (2008) Inhibition of p97-dependent protein degradation by Eeyarestatin I. *J Biol Chem* 283(12):7445–7454.
36. Kruse KB, Brodsky JL, McCracken AA (2006) Autophagy: An ER protein quality control process. *Autophagy* 2(2):135–137.
37. Ryno LM, Wiseman RL, Kelly JW (2013) Targeting unfolded protein response signaling pathways to ameliorate protein misfolding diseases. *Curr Opin Chem Biol* 17(3): 346–352.
38. Wall J, et al. (1999) Thermodynamic instability of human lambda 6 light chains: Correlation with fibrillogenicity. *Biochemistry* 38(42):14101–14108.
39. Klimtchuk ES, et al. (2010) The critical role of the constant region in thermal stability and aggregation of amyloidogenic immunoglobulin light chain. *Biochemistry* 49(45): 9848–9857.
40. Shoulders MD, et al. (2013) Stress-independent activation of XBP1s and/or ATF6 reveals three functionally diverse ER proteostasis environments. *Cell Reports* 3(4): 1279–1292.
41. Chiang WC, Hiramatsu N, Messah C, Kroeger H, Lin JH (2012) Selective activation of ATF6 and PERK endoplasmic reticulum stress signaling pathways prevent mutant rhodopsin accumulation. *Invest Ophthalmol Vis Sci* 53(11):7159–7166.
42. Melnick J, Dul JL, Argon Y (1994) Sequential interaction of the chaperones BiP and GRP94 with immunoglobulin chains in the endoplasmic reticulum. *Nature* 370(6488): 373–375.
43. Feige MJ, Hendershot LM, Buchner J (2010) How antibodies fold. *Trends Biochem Sci* 35(4):189–198.
44. Lachmann HJ, et al. (2003) Outcome in systemic AL amyloidosis in relation to changes in concentration of circulating free immunoglobulin light chains following chemotherapy. *Br J Haematol* 122(1):78–84.

Supporting Information

Cooley et al. 10.1073/pnas.1406050111

SI Materials and Methods

Plasmids and Reagents. The JTO sequence used in this paper is a full-length lambda light chain (LC) using the variable region sequence from the JTO protein (1), fused to the constant region of ALLC (2). The ALLC and JTO sequences were chemically synthesized and purified by Integrated DNA Technologies and supplied in the pIDTSMART vector flanked by a 5′ BamHI and 3′ EcoRI digestion site. ALLC and JTO were inserted into the pENTR1A vector (Invitrogen) using the aforementioned restriction sites, and then ALLC was shuttled into pDEST-14 (for bacterial expression), pTREx-DEST30, pcDNA-DEST40, or pLENTI4/TO vectors as appropriate, using LR clonase II (Invitrogen) recombination. ALLC and JTO were also cloned from the pENTR1A vector into a pCMV1 vector containing a signal sequence and FLAG tag (Sigma) by amplification with the following primers (ALLC: 5′-gaccacaagcttgccagttttatgctggctcagcc and 5′-agctgggtctagatatctcgagtgcg, JTO: 5′-tgctttaagcttaactttatgctgaaccagccgc and 5′-aataaagcggccgctatgaacattctgtaggggccactg) followed by digestion with HindIII and NotI. All constructs were sequenced to confirm their identity. ERSE-Firefly luciferase reporter was cloned into a vector suitable for mammalian cell selection by transferring ERSE-FLuc from ERSE.FLuc.pGL3 (3) into a promoterless pcDNA3.1 vector using Xba1 and Not1 restriction sites.

All compounds were dissolved in sterile dimethyl sulfoxide (DMSO). Thapsigargin (Tg) was obtained from A.G. Scientific. Doxycycline hydrochloride (Dox) and Trimethoprim (TMP) were obtained from Fischer Scientific. MG-132, Bortezomib, Chloroquine, and Eeyarestatin I were obtained from Sigma-Aldrich. GSK2606414 was obtained from Merck Millipore.

Cell Culture and Transfections. HEK293T-Rex (Invitrogen) cells were cultured in complete DMEM (CellGro), and Tet-On ARPE-19 cells (4) were cultured in high-glucose DMEM/F12 50:50 (Gibco) media, both supplemented with 10% FBS (CellGro) and penicillin/streptomycin (CellGro). Transient transfection of ALLC and JTO into HEK293^{DAX} cells was performed by calcium phosphate transfection. Lentiviruses encoding ALLC, ALLC-GLuc, and GLuc were transduced into HEK293T-Rex or ARPE-19 cells using 1–5 mL of virus in media containing 5 mg/mL polybrene. Stable cell lines were selected by culturing in blasticidin (10 μg/mL) and zeocin (50 mg/mL), before characterization. Creation and maintenance of HEK293^{DAX} cells has been described previously (5). HEK293T-Rex cells containing ER stress responsive element-firefly luciferase (ERSE-FLuc) reporter were created by transfection with ERSE.FLuc.pcDNA3.1 by calcium phosphate followed by culturing in geneticin sulfate (G-418, 500 μg/mL) before single colony selection. All cells were cultured under typical tissue culture conditions (37 °C, 5% CO_2).

Virus Production. Vesicular stomatitis virus glycoprotein (VSV-G) pseudotyped lentiviral particles were produced by cotransfecting Lenti-X 293T cells (Clontech) with the structural plasmids necessary for virus production (Rev, RRE, and VSVG) along with the pLentiV5-Dest lentivirus construct. Lenti-X 293T cells were transfected using Fugene-6 (Roche) for 24 h, after which the media was removed and replaced with fresh media. Media containing viral particles was collected at 48 h and again at 72 h posttransfection. Viral particles were concentrated by centrifugation at 40,000 × g for 2 h at ambient temperature. The supernatant was removed, and the pellet containing viral particles was resuspended in Hank's buffered salt solution at 1/100th of the initial volume. Virus was then aliquoted and stored at −80 °C until use. To transduce ARPE-19 or HEK293-TRex cells, the cells were plated at ∼100,000 cells/well in a 12-well plate and infected for 48 h with 1–5 mL of virus in media containing 5 mg/mL polybrene.

Western Blot Analysis. Cells were lysed in 50 mM Tris buffer, pH 7.5 containing 0.1% TritonX (Fisher Scientific) and supplemented with protease inhibitor mixture (Roche). Protein lysate concentrations were normalized by Bradford assays (Bio-Rad). Lysates or media were boiled for 10 min in Laemmli buffer + 100 mM DTT before loading onto SDS-PAGE gel. Proteins were transferred from gel slabs to nitrocellulose, and the Odyssey Infrared Imaging System (Li-Cor Biosciences) was used to detect proteins of interest.

Immunoprecipitation. Cells were washed with PBS and then cross-linked with 0.5 mM Dithiobis(succinimidiyl propionate) (DSP) for 30 min at room temperature. The reaction was quenched by addition of 100 mM Tris pH 7.5, and then radioimmunoprecipitation assay (RIPA) buffer (50 mM Tris pH 7.5, 150 mM NaCl, 0.1% SDS, 1% Triton X-100, 0.5% deoxycholate) containing 10 mM $CaCl_2$ was added for cell lysis. Proteins were immunopurified using anti-FLAG M1 agarose beads (Sigma). Protein was eluted by boiling in Laemmli buffer + 100 mM DTT, and samples were separated by SDS-PAGE as previously described.

Antibodies. Blots were probed with the following primary antibodies: rabbit polyclonal anti-human lambda LC (1:1,000, Bethyl Laboratories A90-112A), mouse monoclonal anti-Grp78 (1:500, Santa Cruz Biotechnology sc-166490), rabbit polyclonal anti-Grp94 (1:1,000, GeneTex GTX103203) and mouse monoclonal anti β-actin (1:10,000, Sigma).

Luciferase Assays. ***GLuc assay.*** Conditioned media (50 μL) was added to a well of a flat-bottomed, black 96-well plate (Costar, Corning Inc.). A solution of 50 nL coelenterazine substrate in 10 μL neat GLuc assay buffer (BioLux Gaussia luciferase assay kit, New England Biolabs) was added to each well, and luminescence activity was measured in a Safire II microplate reader (Tecan).

FLuc reporter assay. HEK293T-Rex cells stably incorporating the ERSE-Firefly Luciferase Reporter were plated ∼20,000 cells per well in flat-bottomed, black 96-well assay plates (Costar, Corning Inc.) overnight before compound administration. Cells were treated with compounds (1−10 μM) for 18 h, and then the plates were equilibrated to room temperature and 50 μL of SteadyLite (PerkinElmer) was added to each well. Luminescence activity was measured in a Safire II microplate reader (Tecan) after 10 min of incubation.

High-throughput screening. ALLC-GLuc and GLuc Tet-ON ARPE19 cells were plated at 5,000 cells/well in flat-bottomed, white, 384-well plates (Costar 3570, Corning) in a total media volume of 20 μL (containing 1 μg/mL Dox to induce expression of the protein of interest). Approximately 6 h after seeding, cells were treated with compounds [10 μM final concentration in DMSO (0.5% final volume)] from the LOPAC dispensed via a Biomek FX pintool instrument (100 nL pintool) and then incubated at 37 °C/5% CO_2 for 24 h. GLuc substrate and buffer (10 nL substrate per well diluted with 2.2 μL of buffer/media) were dispensed directly into the 384-well plate via a BioRAPTR flying reagent dispenser (Beckman Coulter). Luminescence was measured immediately after reagent addition with an EnVision Multilabel Reader (PerkinElmer) using a 100-ms integration time.

Toxicity Assay. HEK293^{DAX} cells transfected with either GFP or ss.FT.ALLC.pCMV1 plasmids were seeded into 96-well plates. After 6 h, a 2× solution of vehicle (DMSO), Tg (500 nM), or Arsenite (100 μM) was added to the cells for 15 h or 24 h. Then 10× Resazurin was added directly to the wells (10 μL) and the plates were incubated for 1 h before measuring fluorescence (excitation 530, emission 590).

Quantitative RT-PCR. Cells were treated as described at 37 °C, harvested by trypsinization, and washed with Dulbecco's PBS (Gibco), and then RNA was extracted using the RNeasy Mini Kit (Qiagen). qPCR reactions were performed on cDNA prepared from 500 ng of total cellular RNA using the QuantiTect Reverse Transcription Kit (Qiagen). The FastStart Universal SYBR Green Master Mix (Roche), cDNA, and appropriate primers purchased from Integrated DNA Technologies (5) were used for amplifications (45 cycles of 2 min at 95 °C, 10 s at 95 °C, 30 s at 60 °C) in an ABI 7900HT Fast Real Time PCR machine. Primer integrity was assessed by a thermal melt to confirm homogeneity and the absence of primer dimers. Transcripts were normalized to the housekeeping gene Rplp2, and all measurements were performed in triplicate. Data were analyzed using the RQ Manager and DataAssist 2.0 softwares (ABI). qPCR data are reported as mean ± 95% confidence interval as calculated in DataAssist 2.0.

LC ELISA. The ELISA was performed in 96-well plates (Immulon 4HBX, Thermo Scientific). Wells were coated overnight at 37 °C with rabbit anti-human lambda LC polyclonal antibody (Bethyl Laboratories) at a 1:1,000 dilution in 50 mM sodium carbonate (pH 9.6). In between all incubation steps, the plates were rinsed extensively with Tris-buffered saline containing 0.05% Tween-20 (TBST). Plates were blocked with 5% nonfat dry milk in TBST for 1 h at 37 °C. ALLC or JTO containing analytes (lysate or conditioned media) were diluted between fivefold and 20-fold in 5% nonfat dry milk in TBST, and 100 μL of each sample was added to individual wells. LC standards ranging from 3 ng/mL to 1,000 ng/mL were prepared from purified human Bence Jones λ LC (Bethyl Laboratories). Plates were incubated at 37 °C for 2 h while shaking. Finally, HRP-conjugated goat anti-human lambda LC antibody (Bethyl Laboratories) was added at a 1:10,000 dilution in 5% nonfat dry milk in TBST, followed by a 2-h incubation of the plates at 37 °C. The detection was carried out with 2,2'-azinobis(3-ethylbenzothiazoline-6-sulfonic acid) (ABTS, 0.18 mg/mL) and 0.03% hydrogen peroxide in 100 mM sodium citrate pH 4.0. Detection solution (100 μL) was added to each well, and the plates were incubated at room temperature. The absorbance was recorded at 405 nm, and the values for the LC standards were fitted to a four-parameter logistic function. LC concentrations were averaged from three independent replicates under each treatment and then normalized to vehicle conditions.

Protein Expression and Purification. LC proteins were expressed as inclusion bodies using a modified version of the protocol described by Rognoni et al. (6). BL21 (DE3) *Escherichia coli* transformed with LC plasmids were grown at 37 °C in ZYP-glucose media and induced overnight with 0.1 mM IPTG. Cells were harvested and lysed, and inclusion bodies were washed three times with phosphate buffered saline (PBS: 10 mM Na_2HPO_4, 1.8 mM KH_2PO_4, 137 mM NaCl, 2.7 mM KCl, pH 7.4) containing 1% Triton-X and once in PBS. The inclusion bodies were dissolved in 6 M guanidine hydrochloride, 5 mM DTT. Insoluble material was removed by centrifugation, and then the protein was refolded by dropwise dilution into 50 mM Tris·Cl (pH 8.5 on ice) containing 5 mM reduced glutathione and 0.5 mM oxidized glutathione. After overnight refolding on ice with stirring, ammonium sulfate was added to 50% saturation and allowed to equilibrate. Insoluble material was removed by centrifugation, and the supernatant, which contained the soluble, folded protein, was filtered and loaded onto a phenyl Sepharose column (GE) equilibrated with 2 M ammonium sulfate. The protein was eluted in 50 mM Tris·Cl pH 8.5. The eluent was concentrated and then purified by size exclusion chromatography on a Superdex 75 column (GE). All LCs eluted at a volume consistent with a dimer of around 45 kDa. Protein purity was assessed by SDS-PAGE; when necessary, the proteins were further purified by anion exchange on a Source 15Q column (GE) at pH 8.5, eluting with a 0–0.5 M NaCl gradient. Protein solutions were filter sterilized and stored at 4 °C and dialyzed into appropriate buffers for further analysis. Protein concentrations are given in milligrams per milliliter, to avoid ambiguity between monomer and dimer concentrations.

Circular Dichroism Spectroscopy. Proteins were dialyzed into 50 mM sodium phosphate buffer, pH 7, and diluted to 0.2 mg/mL. CD spectra were recorded on an Aviv 420SF spectrapolarimeter at 25 °C with a resolution of 1 nm. Aliquots of the protein stocks were unfolded in 8 M urea, and their tryptophan fluorescence intensity (excitation 280 nm, emission 300–400 nm) used to normalize the CD spectra. This allows direct comparison of the secondary structure content of the proteins, and bypasses inaccuracies in determining their concentration by absorbance spectroscopy. Mean residue ellipticity $[\Theta]_{MRE}$ was calculated with the formula:

$$[\Theta]_{MRE} = \frac{\Theta_{obs} \times M_r/(n-1)}{c \times d}.$$

Θobs is the measured ellipticity in millidegrees, M_r is the molecular weight of the protein, n is its number of amino acids, c is its concentration in milligrams per milliliter, and d is the cuvette pathlength in millimeters.

Urea Denaturation Titrations. LC proteins were incubated overnight at 25 °C in 50 mM sodium phosphate buffer, pH 7, containing varying urea concentrations. Protein concentration was approximately 0.1 mg/mL. Intrinsic tryptophan fluorescence was measured on an Aviv ATF 105 spectrofluorimeter at 25 °C, using an excitation wavelength of 280 nm and recording emission spectra between 300 nm and 400 nm. Each LC monomer has three tryptophan residues, two of which are quenched in the native state by packing against the disulfide bond in each domain. To assess spectral changes as a function of urea concentration, we calculated the average wavelength, <λ> (7):

$$\langle\lambda\rangle = \frac{\sum_i \lambda_i \cdot I_i}{\sum_i I_i}$$

where λ and I are the wavelength and intensity at that wavelength, calculated across the emission spectrum. The data were fit to a two-state equilibrium unfolding equation (8):

$$\frac{(a+bx)e^{\frac{G-mx}{RT}} + (c+dx)}{1+e^{\frac{G-mx}{RT}}}$$

where x is the urea concentration (M), G is the free energy of unfolding (kJ/mol), m is the denaturant dependence of the unfolding reaction (kJ/mol/M), R is the ideal gas constant, T is the temperature in K, a and c are the fluorescence of the folded and unfolded states, and b and d are the denaturant dependence of the fluorescence of the folded and unfolded states, respectively. We were unable to quantitatively refold either LC protein from its urea-denatured state, as assessed by tryptophan fluorescence (Fig. S3*A*). This may be due to aggregation or misfolding of the dimer. Therefore, we assume that the protein is not truly at equilibrium, so the stabilities measured here should be treated with caution. We report only the unfolding midpoint urea concentration, C_m, calculated from the fit by $m \times G$.

Aggregation Kinetics. ALLC was filtered with a 0.22-μm syringe filter then serially diluted 1.2-fold from 1.5 mg/mL to 0.25 mg/mL concentration in PBS containing 0.5 M $MgSO_4$ (9). The protein solutions were aliquoted onto a 96-well microplate in triplicate, and the plate was sealed with Crystal Clear tape (Hampton). Aggregation was assessed by turbidity. The plate was incubated at 44 °C, and absorbance at 405 nm was measured in a Molecular Devices SpectraMax 250 plate reader (44 °C is the maximum temperature that the plate reader can maintain). Incubation at 37 °C or without $MgSO_4$ for up to 8 d did not produce aggregates. Aggregation t_{50} was determined from the individual absorbance traces by determining the average initial and final absorbances and then fitting to a double-exponential function and finding the root of the fit equation at the midpoint of the initial and final absorbance values. We were unable to fit the traces to a mechanistic model, which prevented a more detailed analysis of lag times or growth rates.

1. Wall J, et al. (1999) Thermodynamic instability of human lambda 6 light chains: Correlation with fibrillogenicity. *Biochemistry* 38(42):14101–14108.
2. Arendt BK, et al. (2008) Biologic and genetic characterization of the novel amyloidogenic lambda light chain-secreting human cell lines, ALMC-1 and ALMC-2. *Blood* 112(5):1931–1941.
3. Yoshida H, Haze K, Yanagi H, Yura T, Mori K (1998) Identification of the *cis*-acting endoplasmic reticulum stress response element responsible for transcriptional induction of mammalian glucose-regulated proteins. Involvement of basic leucine zipper transcription factors. *J Biol Chem* 273(50):33741–33749.
4. Hulleman JD, Brown SJ, Rosen H, Kelly JW (2013) A high-throughput cell-based Gaussia luciferase reporter assay for identifying modulators of fibulin-3 secretion. *J Biomol Screen* 18(6):647–658.
5. Shoulders MD, et al. (2013) Stress-independent activation of XBP1s and/or ATF6 reveals three functionally diverse ER proteostasis environments. *Cell Reports* 3(4):1279–1292.
6. Rognoni P, et al. (2013) A strategy for synthesis of pathogenic human immunoglobulin free light chains in *E. coli*. *PLoS ONE* 8(9):e76022.
7. Royer CA, Mann CJ, Matthews CR (1993) Resolution of the fluorescence equilibrium unfolding profile of trp aporepressor using single tryptophan mutants. *Protein Sci* 2(11):1844–1852.
8. Maxwell KL, et al. (2005) Protein folding: Defining a "standard" set of experimental conditions and a preliminary kinetic data set of two-state proteins. *Protein Sci* 14(3): 602–616.
9. McLaughlin RW, De Stigter JK, Sikkink LA, Baden EM, Ramirez-Alvarado M (2006) The effects of sodium sulfate, glycosaminoglycans, and Congo red on the structure, stability, and amyloid formation of an immunoglobulin light-chain protein. *Protein Sci* 15(7):1710–1722.

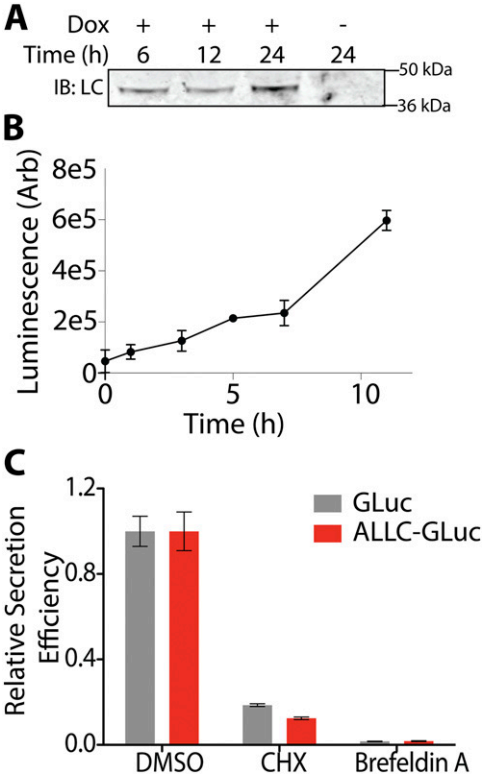

Fig. S1. ALLC-GLuc is efficiently secreted from mammalian cells. (*A*) Immunoblot of media conditioned on HEK293T-Rex cells transiently transfected with Doxycycline (Dox)-inducible ALLC-GLuc for the indicated time. Dox (1 μg/mL) was added for 24 h, and then the media was replaced with fresh media and secreted ALLC was measured by SDS-PAGE/immunoblot at the indicated time. (*B*) Plot showing the GLuc luminescence of media conditioned on HEK293T-Rex cells transiently transfected with Dox-inducible ALLC-GLuc for the indicated time. Dox (1 μg/mL) was added for 24 h, and then the media was replaced with fresh media and secreted ALLC was measured by GLuc luminescence assay at the times indicated. Error bars show SEM for $n = 3$. (*C*) Graph showing the secretion of ALLC-GLuc or GLuc from HEK293T-Rex cells transiently transfected with Dox-inducible ALLC-GLuc or Dox-inducible GLuc. Dox (1 μg/mL) was added to the cells for 15 h, and then the media was replaced by media containing vehicle (DMSO), cycloheximide (CHX, 5 μM), or Brefeldin A (5 μg/mL) as indicated. After 6 h incubation, secretions of ALLC-GLuc and GLuc were measured by GLuc luminescence assay, and values were normalized to vehicle control. Error bars represent SEM for biological replicates ($n = 3$).

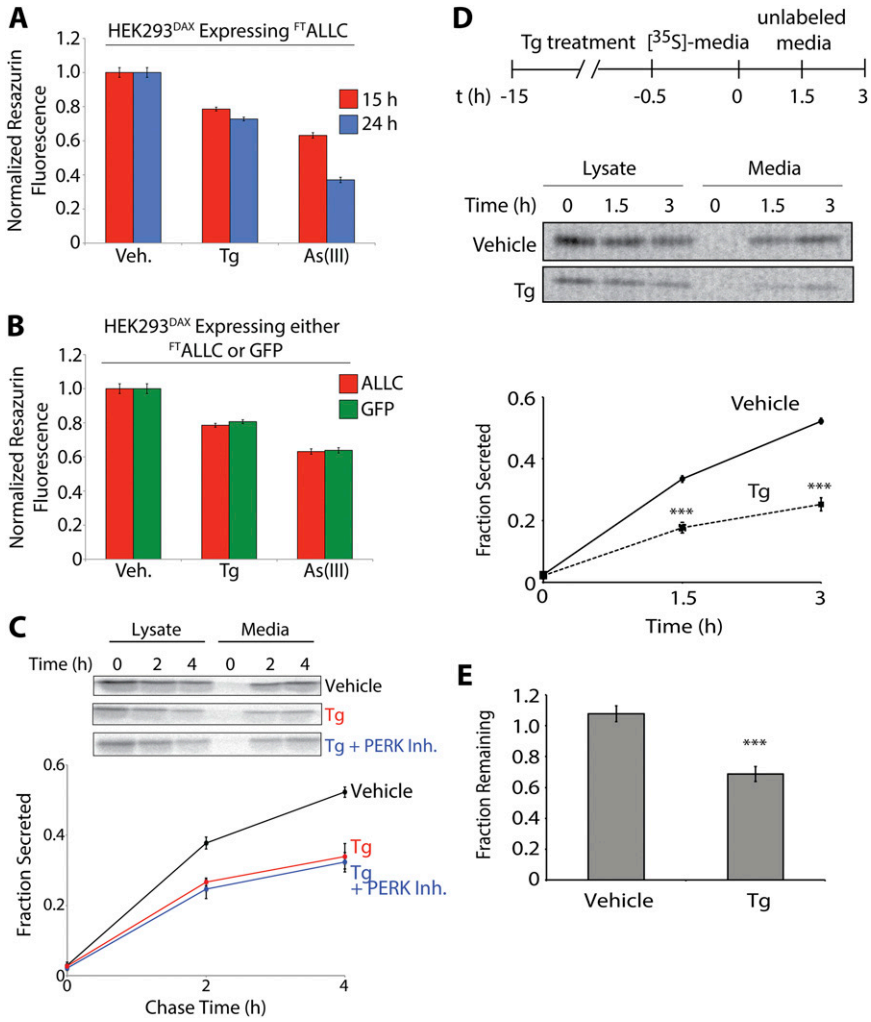

Fig. S2. Tg reduces the secretion and increases the degradation of destabilized ALLC. (*A*) Bar graph showing the viability of HEK293^{DAX} cells treated with thapsigargin (Tg; 500 nM) for 15 or 24 h measured by resazurin fluorescence. Highly toxic arsenite [As(III); 100 μM] was included as a control. These results demonstrate that the treatment of HEK293^{DAX} cells with Tg for 15–24 h does not dramatically reduce the viability of these cells. Error bars show SEM for biologic replicates ($n = 3$). (*B*) Bar graph showing the viability of HEK293^{DAX} cells expressing ^{FT}ALLC or GFP (as a control) treated with thapsigargin (Tg; 500 nM) for 15 (red) or 24 (blue) h measured by resazurin fluorescence. Highly toxic arsenite (As(III); 100 μM) was included as a control. These results demonstrate that the overexpression of ^{FT}ALLC does not significantly increase the sensitivity of HEK293^{DAX} cells to Tg-induced ER stress. Error bars show SEM for biologic replicates ($n = 3$). (*C*) Autoradiogram and graph depicting the fraction secreted of [^{35}S]-labeled ^{FT}ALLC immunopurified with M1 FLAG antibody from media and lysates collected from transfected HEK293^{DAX} cells following a 1-h pretreatment with GSK2606414 (30 nM) and then a 15-h preactivation with Tg (500 nM). GSK2606414 was added during the Tg incubation as well. Fraction secreted was calculated by normalizing the [^{35}S] signal in the media at each time point to the total amount of labeling at t = 0 as described in *Materials and Methods*. Error bars represent SEM from biological replicates ($n = 2$). (*D*) Autoradiogram and graph depicting the fraction secreted of [^{35}S]-labeled ALLC immunopurified with anti-human lambda LC antibody from media and lysates collected from transfected HEK293^{DAX} cells following a 15-h preactivation with Tg (500 nM). The labeling protocol is shown. Fraction secreted was calculated by normalizing the [^{35}S] signal in the media at each time point to the total amount of labeling at t = 0 as described in *Materials and Methods*. Error bars represent SEM from biological replicates ($n = 6$). ***$P < 0.005$. (*E*) Graph depicting total [^{35}S]-labeled ALLC remaining at 3 h in HEK293T-Rex cells following a 15-h pretreatment with 500 nM Tg ($n = 6$). The fraction remaining was calculated as described in *Materials and Methods*. ***$P < 0.005$.

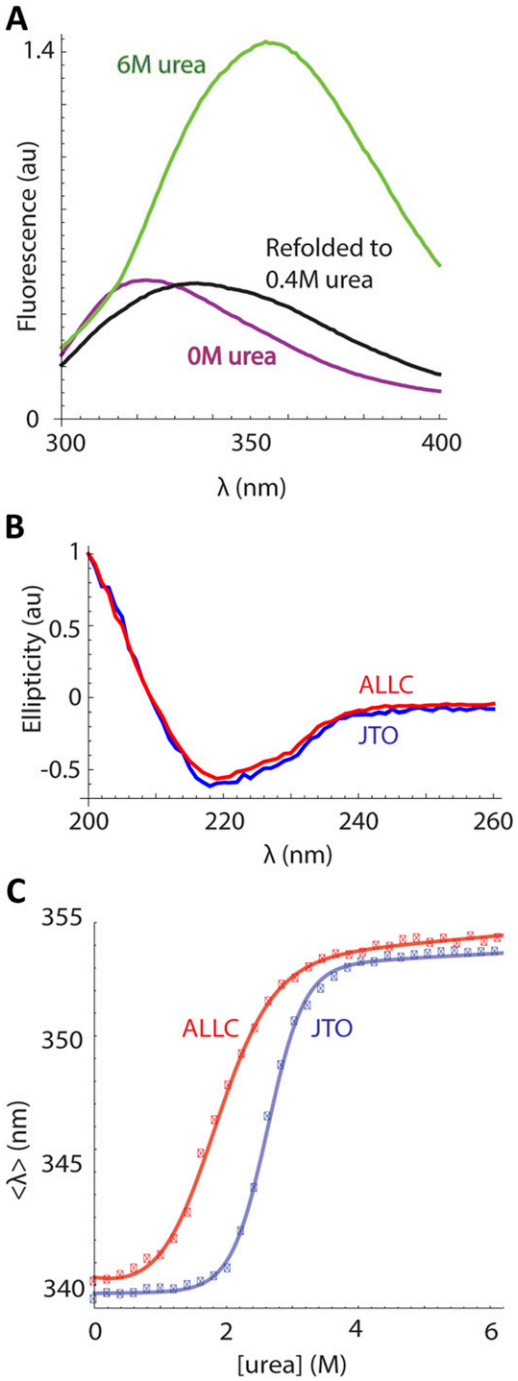

Fig. S3. Stability of recombinant ALLC and JTO. (*A*) Intrinsic tryptophan fluorescence spectra of recombinant ALLC in native (purple trace) and denaturing (green trace, 6 M urea) conditions showing the characteristic fluorescence quenching by the disulfide bonds in each domain. Protein refolded from 6 M urea by dilution to 0.4 M urea under nonoxidizing conditions (black trace) did not regain a native-like fluorescence spectrum, demonstrating that recombinant ALLC unfolding is not reversible. (*B*) Circular dichroism spectra of ALLC (red) and JTO (blue) show characteristic and indistinguishable β-sheet structures. (*C*) Urea titrations of ALLC (red) and JTO (blue) show that JTO has a higher apparent stability than ALLC. Spectroscopic data were measured in 50 mM sodium phosphate buffer and urea concentrations ranging from 0 M to 6 M at pH 7, 25 °C.

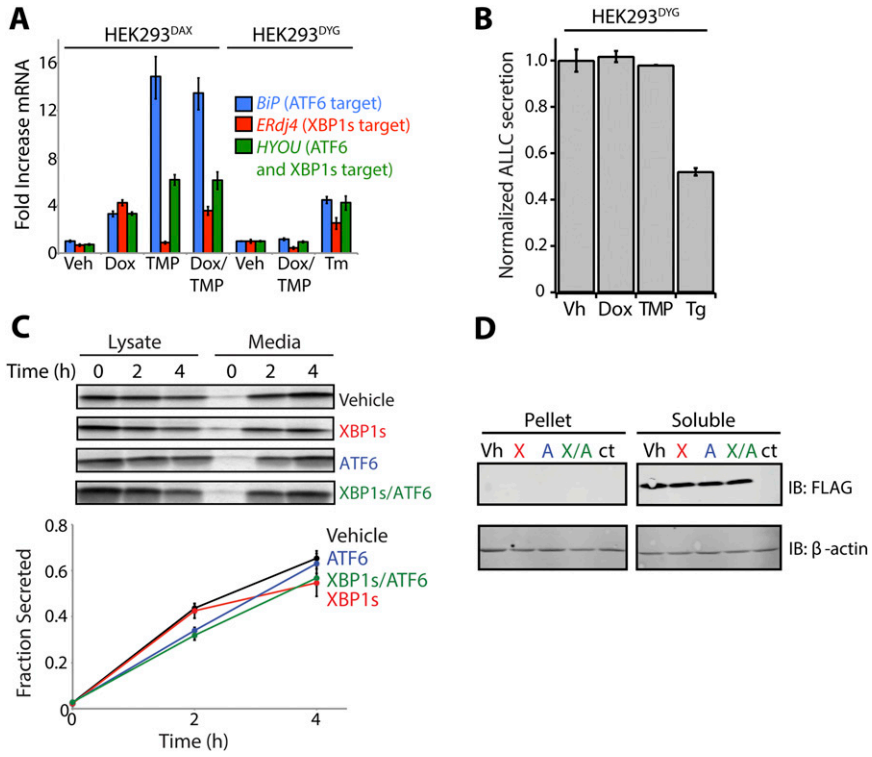

Fig. S4. Stress-independent activation of XBP1s and/or ATF6 in HEK293^{DAX} cells does not significantly influence secretion of the stable LC JTO. (*A*) qPCR analysis of XBP1s and ATF6 target genes in HEK293^{DAX} and HEK293^{DYG} cells following a 15-h treatment with Dox (1 μg/mL), TMP (10 μM), or the ER stressor tunicamycin (Tm, 1 μg/mL). Data are shown normalized to vehicle-treated HEK293^{DYG} cells. Error bars show ±95% confidence interval for $n = 3$. HEK293^{DAX} cells stably express DHFR-ATF6 and Dox-inducible XBP1s (5). HEK293^{DYG} cells stably express DHFR-YFP and Dox-inducible GFP (5). Thus, we only observe the selective induction of XBP1s and/or ATF6 target genes in HEK293^{DAX} cells treated with the appropriate activating ligand, clearly indicating our ability to sensitively activate the XBP1s and/or ATF6 transcriptional programs in HEK293^{DAX} cells. (*B*) ALLC levels by ELISA in HEK293^{DYG} cells expressing ^{FT}ALLC following a 15-h treatment with Dox (1 μg/mL), TMP (10 μM), or thapsigargin (Tg, 500 nM). Error bars represent SEM from biological replicates ($n = 3$). These results show that the reduction in ^{FT}ALLC secretion afforded by stress-independent XBP1s and/or ATF6 activation in HEK293^{DAX} cells requires the activity of these UPR-associated transcription factors. (*C*) Representative autoradiogram and quantification of [^{35}S]-labeled ^{FT}JTO immunopurified from media and lysates collected from transfected HEK293^{DAX} cells following a 15-h preactivation of XBP1s (Dox; 1 μg/mL), ATF6 (TMP; 10 μM), or both. Fraction secreted was calculated as described in *Materials and Methods*. Error bars represent SEM from biological replicates ($n = 3$). (*D*) Immunoblots measuring soluble and insoluble (pellet) levels of ^{FT}ALLC or untagged ALLC (Ct) following a 15-h preactivation of XBP1s (X; Dox; 1 μg/mL), ATF6 (D; TMP; 10 μM), or both (X/A). Lysates and pellets were harvested from cells and the protein from the pellets extracted in 8 M urea before SDS-PAGE and immunoblotting.

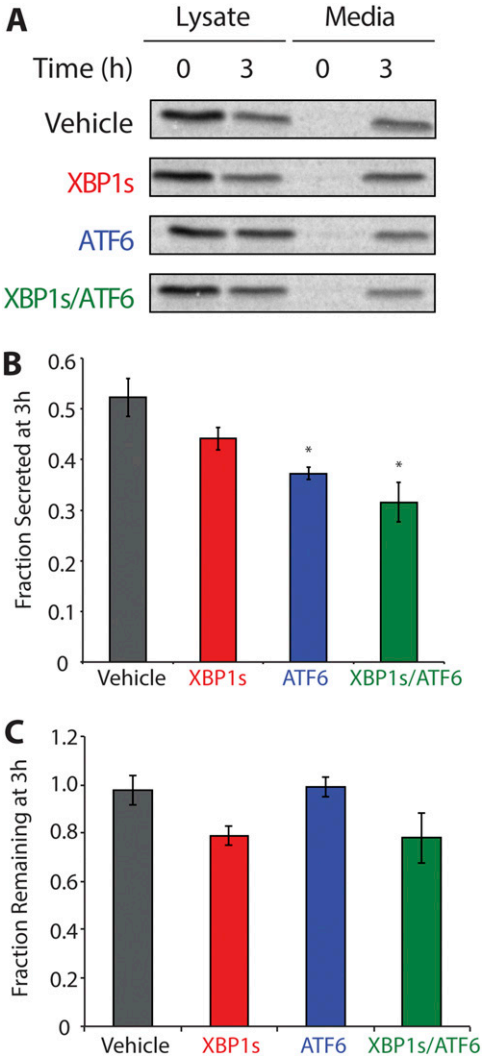

Fig. S5. XBP1s and ATF6 similarly affect the secretion and degradation of untagged ALLC. (*A*) Autoradiogram of [^{35}S]-labeled ALLC immunopurified from media and lysates collected from transfected HEK293^{DAX} cells following a 15-h preactivation of XBP1s (Dox; 1 μg/mL), ATF6 (TMP; 10 μM), or both. (*B*) Graph depicting the fraction secreted after 3 h of chase in *A*. Fraction secreted was calculated as described in *Materials and Methods*. *$P < 0.05$. (*C*) Graph depicting total [^{35}S]-labeled ^{FT}ALLC remaining at 3 h in *A*. The fraction remaining was calculated as described in *Materials and Methods*. All error bars represent SEM from biological replicates ($n = 3$).

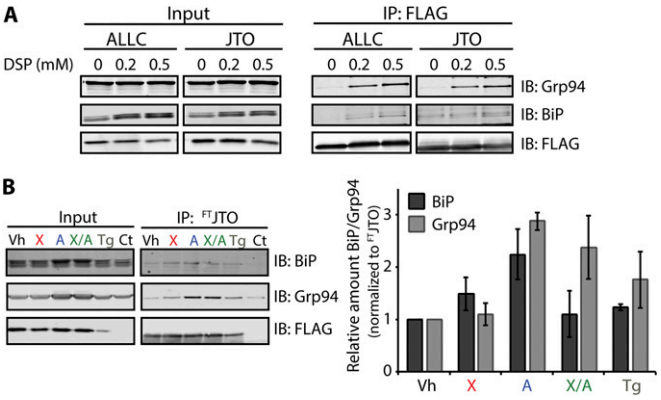

Fig. S6. Cross-linking allows for the quantification of intracellular interactions between LC proteins and ER chaperones. (*A*) Immunoblots of SDS-PAGE gels showing the inputs and FLAG immunopurifications of ^{FT}ALLC and ^{FT}JTO from HEK293^{DAX} cells treated in situ with increasing concentrations of the reversible cross-linker DSP [dithiobis(succinimidiyl propionate)]. The cross-linking and FLAG immunopurifications were performed as described in *SI Materials and Methods* and washed with high-detergent RIPA buffer. Note that the ER chaperones BiP and GRP94 are only recovered in our FLAG immunopurifications performed on lysates prepared from DSP-cross-linked cells, demonstrating that our cross-linking protocol allows for the recovery of intracellular interactions between LCs and ER chaperones without the complications arising from postlysis artifacts. (*B*) Immunoblot and quantification for FLAG immunopurifications of ^{FT}JTO isolated from HEK293^{DAX} cells following a 15-h treatment with Tg (500 nM) or preactivation of XBP1s (X), ATF6 (A), or both (X/A). The bar graph shows the recovery of BiP and GRP94 from these ^{FT}JTO immunopurifications quantified by comparing the signal for each of these ER chaperones under various conditions to vehicle and normalizing to the recovered ^{FT}JTO. HEK293^{DAX} cells expressing untagged ALLC was used as a control (Ct). All error bars represent SEM from biological replicates (n = 3).

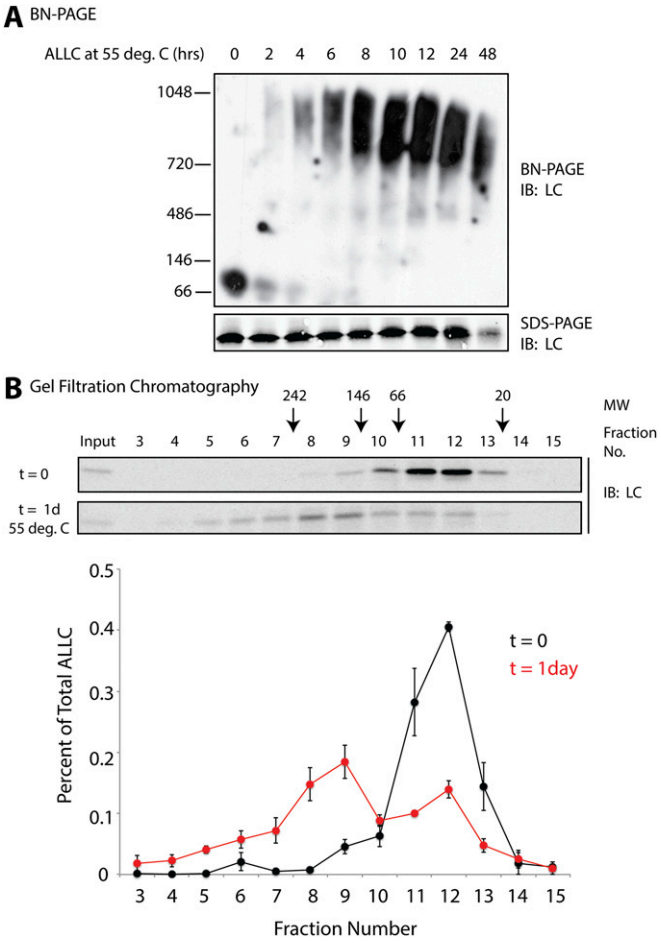

Fig. S7. ALLC aggregates into soluble oligomers in conditioned media upon heating. (*A*) Immunoblots of BN-PAGE and SDS-PAGE gels from media conditioned on HEK293 cells expressing ^{FT}ALLC following incubation at 55 °C for the indicated time. (*B*) Immunoblot and quantification from gel filtration fractions of media conditioned on HEK293 cells expressing ^{FT}ALLC following 24-h incubation at 55 °C. Fractions (1 mL) were collected and analyzed by SDS-PAGE and immunoblot for LC relative to MW standards. Quantification of the immunoblots is shown below. Percent ALLC protein represents the fraction ALLC detected in each fraction relative to the total ALLC detected in each run. Error bars represent SEM from biological replicates (n = 3).

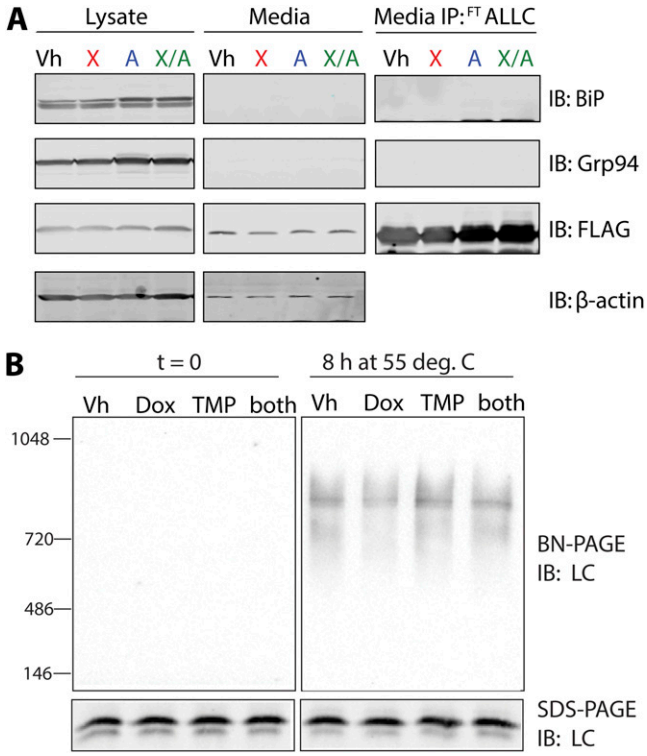

Fig. S8. Doxycycline and TMP do not affect ^{FT}ALLC aggregation in media conditioned on HEK293^{DYG} cells. (*A*) Immunoblot of lysates, media, and FLAG immunopurifications of the media prepared from HEK293^{DAX} cells expressing ^{FT}ALLC following a 15-h preactivation of XBP1s (X; Dox, 1μg/mL), ATF6 (A; TMP, 10 μM), or both XBP1s and ATF6 (X/A). We do not recover the ER chaperones BiP or GRP94 in the FLAG immunopurifications, demonstrating that the reduced aggregation of secreted ^{FT}ALLC cannot be attributed to the activity of increased extracellular populations of these ER chaperones. (*B*) Immunoblots of BN-PAGE and SDS-PAGE gels of media conditioned on HEK293^{DYG} cells transiently expressing ^{FT}ALLC following a 16-h treatment with Dox (1 μg/mL), TMP (10 μM), or both. After 16-h incubation of the media with ALLC-expressing cells, the media was incubated at 55 °C for 8 h, and soluble aggregates were measured by BN-PAGE.